symmetry

MDPI

Article

Liouville Theory for Fully Analytic Studies of Transverse Beam Dynamics in Laser-Plasma Ion Accelerators

Alessandro Curcio [1,*], Jon Imanol Apiñaniz Aginako [1], Teresa Cebriano Ramírez [1], Michael Ehret [1], Berkahoum Kebladj [2], Antonia Morabito [1], Alberto Pérez Delgado [1], Carlos Salgado López [1], Luca Volpe [1] and Giancarlo Gatti [1]

[1] Centro de Laseres Pulsados (CLPU), Edificio M5. Parque Científico. C/Adaja, 8., 37185 Villamayor, Spain
[2] Fundamental Physics Department, University of Salamanca, 37008 Salamanca, Spain
* Correspondence: acurcio@clpu.es

Abstract: The exact solution of the Liouville equation expressed in terms of exponential operators can describe the phase space evolution of particle beams in transport lines. In this paper, we generalize the solution of the above equation for the case of beam losses induced by apertures and for particle beams with large spreads in the momentum space. We discuss the applicability of such approach to ion beams produced by high-intensity lasers interacting with critical plasmas, based on the comparison between theoretical findings and measurements.

Keywords: Liouville equation; laser-plasma accelerators; beam dynamics

Citation: Curcio, A.; Apiñaniz Aginako, J.I.; Cebriano Ramírez, T.; Ehret, M.; Kebladj, B.; Morabito, A.; Pérez Delgado, A.; Salgado López, C.; Volpe, L.; Gatti, G. Liouville Theory for Fully Analytic Studies Transverse Beam Dynamics in Laser-Plasma Ion Accelerators. *Symmetry* **2022**, *14*, 1875. https://doi.org/10.3390/sym14091875

Academic Editors: Eugene Oks and Stefano Profumo

Received: 10 August 2022
Accepted: 6 September 2022
Published: 8 September 2022

1. Introduction

It is undeniable that particle accelerators have nowadays a significant societal impact. They not only find application in fundamental physics, for exploring the origin and the very nature of our universe reaching regimes of interaction otherwise not possible on our planet [1], but they are also exploited for medical purposes [2] (production of radioisotopes, hadrontherapy, radiotherapy, diagnostic imaging, etc.), industrial applications [3] (sealing milk cartons tightly, making chips for computers, etc.), and others [4,5]. Several laser-plasma acceleration techniques have been demonstrated during the past decades [6]. Laser-based accelerators have the advantage, compared to machines based on radio frequency (RF), to be compact, and in most cases, more cost-effective. The generation of fast ions via high-intensity lasers ($I >> 10^{18}$ W/cm^2) commonly occurs through the interaction of such lasers with solid targets, i.e., foils of solid materials. The head of the laser pulse ionizes the surface of such foils, creating a critical plasma. The transition between the underdense and the overderdense plasma is very sharp, on the scale of a fraction of laser wavelength. In the target normal sheath acceleration (TNSA) scheme, the one relevant for the present paper, laser energy is coupled into fast electrons that propagate inside the foil finally escaping from the rear of the latter. The charge imbalance created at the rear of the target is responsible for the generation of strong electric fields that accelerate protons and ions. The TNSA mechanism has been extensively studied and well understood [7]. The ion beams produced in the latter scheme have been characterized in many experiments. Laser-plasma accelerator physicists are eventually finding solutions for beam transport, manipulation, and use in recent times. Energy selection has been demonstrated, by means of dipole magnets coupled to slits [8,9], as well as beam focusing strategies, mostly based on solenoids and/or quadrupole magnets [10–16]. Transported and focused beams have been already used for tumor irradiation (not yet on humans) and can be exploited for diverse applications involving irradiation [17]. Indeed, proton and ion beams are one of the best candidates for local irradiation due to their intrinsic properties of energy loss in dense matter, summarized in the concept of Bragg peak [18]. Beam transport lines must be properly designed, "sewn on" the beams that must be propagated and/or manipulated.

In order to achieve the desired performances, in terms of charge transport and phase space selection and control, simulation methods and/or calculations are needed. Several well-established codes, a few of them commercial, can be found for the tracking of the particle states under the action of external fields, finally allowing a reconstruction of the phase space evolution of particle beams [19,20]. Analytic approaches, as matrix optics or beam envelope equations, are also commonly used, normally carrying a poorer degree of approximation. The solution of the Liouville equation corresponds to the evolution of the phase space density, thus it is a more general approach than the beam envelope equations: in fact the beam envelope equations describe the evolution of the statistical momenta of the phase space density rather than the density itself. In a previous paper, we have demonstrated that the analytic solution of the Liouville equation can be properly used to fully describe the phase spaces of particle beams propagating in external fields [21]. The application of such approach has been demonstrated for the case of electron beams compressed in magnetic chicanes and for the description of the longitudinal dynamics (i.e., the evolution of the bunch length and of the energy spread) of the same beams in linear RF accelerators. In the same work, we anticipated how to use the Liouville formalism for studies of transverse dynamics (i.e., the evolution of the beam envelopes) but without providing any experimental comparison and neglecting beam losses. In the present paper, we extend the previous model to the case of beam losses and chromatic beam transport, significant in laser-plasma accelerators, and furthermore we compare the theoretical results with experimental measurements, to open a discussion about the pros and cons of using the Liouville approach instead of others.

2. Methods

Let us consider a beam of protons at the kinetic energy E propagating along z. A beam of particles is characterized by a certain degree of directionality, this is why it is possible to identify a main direction of propagation, even for the case that the divergence of the beam is rather large. The horizontal and vertical propagation angles for any particle in the beam are defined, in general, as $\vec{\theta} = \{\arctan(v_x/v_z), \arctan(v_y/v_z), 0\}$, where $\vec{v}$ is the velocity vector of the same particle. The particles propagate under a field of external forces $\vec{F}$. Please notice that the $\vec{r} - \vec{\theta}$ space is more commonly known as trace-space instead of phase-space. Studying the transverse dynamics of the particle beam with respect to the beam barycenter the time t and the z-coordinate can be related through the mean beam velocity $\bar{v}$. The results shown in this paper refer to the transverse beam dynamics, i.e., the trace-space density is always time-integrated; therefore, the Liouville equation for the evolution of the beam spatial-angular distribution $\rho_\perp^E$ (at fixed energy E) can be written as below:

$$\frac{d\rho_\perp^E}{dz} = \frac{\partial \rho_\perp^E}{\partial z} + \vec{\theta} \cdot \vec{\nabla}_{\vec{r}_\perp} \rho_\perp^E + \frac{2\vec{F}}{E} \cdot \vec{\nabla}_{\vec{\theta}} \rho_\perp^E = \rho_\perp^E \frac{\partial \log A(x,y;z)}{\partial z} \tag{1}$$

Equation (1) is a generalization of the equation derived in Ref. [21] to the case of beam losses due to apertures along the beam propagation axis. The aperture function is $A(x,y;z)$ is constantly equal to 1 at $z = 0$ and it is a step-function of the transverse plane $x - y$ for $z > 0$. In other words $A = 1$, for all particles entering the apertures and $A = 0$ outside the apertures. The derivation of Equation (1) is reported in Appendix A. The Liouville operator for the particles occupying the status of kinetic energy E is defined as:

$$\bar{L}_\perp^E = -\vec{\theta} \cdot \vec{\nabla}_{\vec{r}_\perp} - \frac{2\vec{F}}{E} \cdot \vec{\nabla}_{\vec{\theta}} \tag{2}$$

Given the above, the solution of Equation (1) is found:

$$\rho_\perp^E(x,y,\theta_x,\theta_y;z) = A(x,y;z) e^{\int_0^z dz \bar{L}_\perp^E} \rho_\perp^E(x,y,\theta_x,\theta_y;0) \tag{3}$$

which, using the definition at Equation (2), can be recast into:

$$\rho_{\perp}^{E}(x,y,\theta_x,\theta_y;z) = A(x,y;z)e^{-\int_0^z dz\vec{\theta}\cdot\vec{\nabla}_{\vec{r}_\perp} - \int_0^z dz\frac{2\vec{F}}{E}\cdot\vec{\nabla}_{\vec{\theta}}}\rho_{\perp}^{E}(x,y,\theta_x,\theta_y;0) \tag{4}$$

As shown in Ref. [22] the exponential operator in Equation (4) can be recognized as a unitary displacement operator, thus obtaining the final expression for the solution of Equation (1):

$$\rho_{\perp}^{E}(x,y,\theta_x,\theta_y;z) = A(x,y;z)\rho_{\perp}^{E}\left(x - \int_0^z dz\theta_x, y - \int_0^z dz\theta_y, \theta_x - \int_0^z dz\frac{2F_x}{E}, \theta_y - \int_0^z dz\frac{2F_y}{E}; 0\right) \tag{5}$$

The power of the above solution is that knowing the single-particle dynamics, i.e., the functions $\theta_{x,y}(z)$, allows the description of the whole beam in the trace-space at any position along the beamline. In fact, the evolved trace-space density is calculated upon the initial trace-space density after the implementation of dynamical shifts in the argument of the function, which in turn depend on the single-particle dynamics. The expressions for the particle trajectories relevant to this paper are given in Appendix B. The trace-space density $\rho_{\perp}^{E}$ contains information only of the particles with kinetic energy E so the full beam information is retrieved after integration on the beam energy spectrum. We follow Ref. [23] for representing the thermal spectrum (the temperature parameter is T) of protons accelerated during laser–plasma interactions at high-intensity.

$$\rho_E(E) = \frac{e^{-\sqrt{\frac{2E}{T}}}}{\sqrt{2ET}} \tag{6}$$

The transverse beam profile at the plane z is therefore defined self-consistently as:

$$P(x,y;z) = \int\int\int \rho_E(E)\rho_{\perp}^{E}(x,y,\theta_x,\theta_y;z)d\theta_x\theta_y dE \tag{7}$$

The presented theory has been used to interpret the experimental data acquired within an experimental campaign on the PW VEGA 3 laser system of Centro de Laseres PUlsados (CLPU) in Salamanca, Spain [24]. During the campaign, ion beams have been generated via the TNSA mechanism and transported through a triplet of permanent quadrupole magnets. The experimental setup is reported in Figure 1.

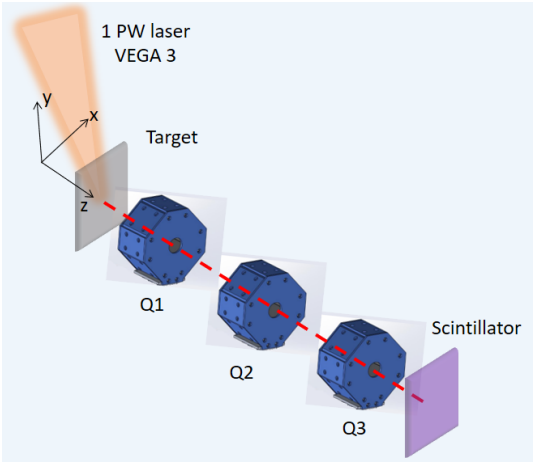

Figure 1. Experimental setup. The dashed line indicates the proton propagation direction.

The corresponding force field is $F_x = +qgx(z)\sqrt{2E/M}$, $F_y = -qgy(z)\sqrt{2E/M}$ inside the first quadrupole $Q1$, then $F_x = -qgx(z)\sqrt{2E/M}$, $F_y = +qgy(z)\sqrt{2E/M}$ inside $Q2$, the force field in the third quadrupole $Q3$ is the same as in $Q1$, and finally is zero elsewhere. The force field has been approximated to a linear one to keep the model to a fully analytical

level, in fact with such a choice the single-particle dynamics can be solved in a closed form. The drawbacks of this strategy is that non-linear aberrations induced by the focusing system cannot be properly represented; however, for the purposes of the present paper such a degree of approximation has been sufficient. The proton charge has been defined as q, while its mass as M. The edge-effects of the field, are renormalized within the effective gradient parameter $g = 40.8$ T/m. Non-conservative forces due to space charge are neglected because the beam is studied well after the Coulomb explosion: the 3D beam expansion makes the internal forces negligible already a few mm after the target. The target is a 6 μm thick Al foil. The laser impinges at 10° with respect to the normal to the target. The ion spectrum before the quadrupole system has been characterized by means of a Thomson parabola [25]. After the observation of Carbon ion species, the latter have been stopped by means of a Pokalon thin foil (13 μm), which resulted in a proton deceleration <0.1 MeV in the spectral range of interest. The focused beam profile has been detected by means of a $BC - 400$ plastic scintillator, 5 mm thick.

3. Results

The first result that we show is the comparison between the measured and calculated transverse beam profiles at the plane of the scintillator. The distance between the target and the first quadrupole is 15 mm; the distance between $Q1$ and $Q2$ is 65 mm, while the distance between $Q2$ and $Q3$ is 85 mm. The quadrupole length is 100 mm for all the quadrupole magnets and the scintillator is at 130 mm after $Q3$. Figure 2 shows the experimental beam profile on the left and the one calculated by means of Equation (7) on the right. The color scale is in arbitrary units, but a discussion on the bunch charge will be given later on in the text.

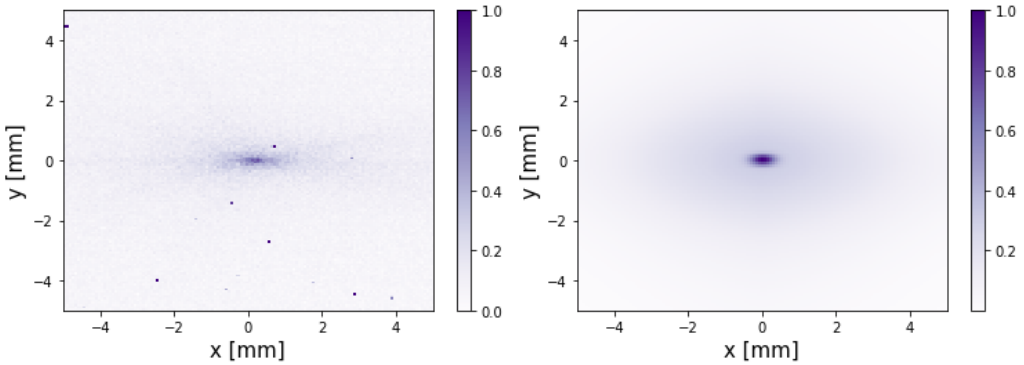

Figure 2. Proton focus. **Left**: experimental measurement. **Right**: solution of the Liouville equation.

In order to obtain the image on the right, we have assumed a temperature of 0.6 MeV for reasons that will be clearer hereafter. Moreover, the initial transverse beam size at the source has been chosen 100 μm both along x and y, considering this value as the rms of a symmetric bigaussian distribution. We have observed in our simulations that an initial value of the beam size as the one adopted or smaller does not have a strong influence on the beam dynamics, i.e., the corresponding calculations do not show different results. The initial beam divergence, previously characterized with the multi-pin-hole Thomson parabola, has been set to 20° rms in both transverse directions. The agreement shown in Figure 2 further confirms the validity of our initial parameters. Concerning the choice of temperature for the profile calculation at the plane of the scintillator, this has been dictated by two experimental constraints: one is the minimization of the differences between the measured and calculated horizontal and vertical beam profiles and the other is the direct measurement of beam temperature from the proton spectra. Figure 3 shows the measured transverse beam profiles compared to the ones calculated for different beam temperatures. It is evident that the best matching between theory and experiment is found for a beam temperature of 0.6 MeV. The used algorithm for finding the best matching has been a

minimization algorithm on the norm of the difference vectors $|\vec{P}_{m,x} - \vec{P}_{s,x}|$ and $|\vec{P}_{m,y} - \vec{P}_{s,y}|$ where $\vec{P}_{m,i}$ and $\vec{P}_{s,i}$ are the measured and simulated profiles, respectively, with $i = x, y$ according to the considered projection (horizontal and vertical).

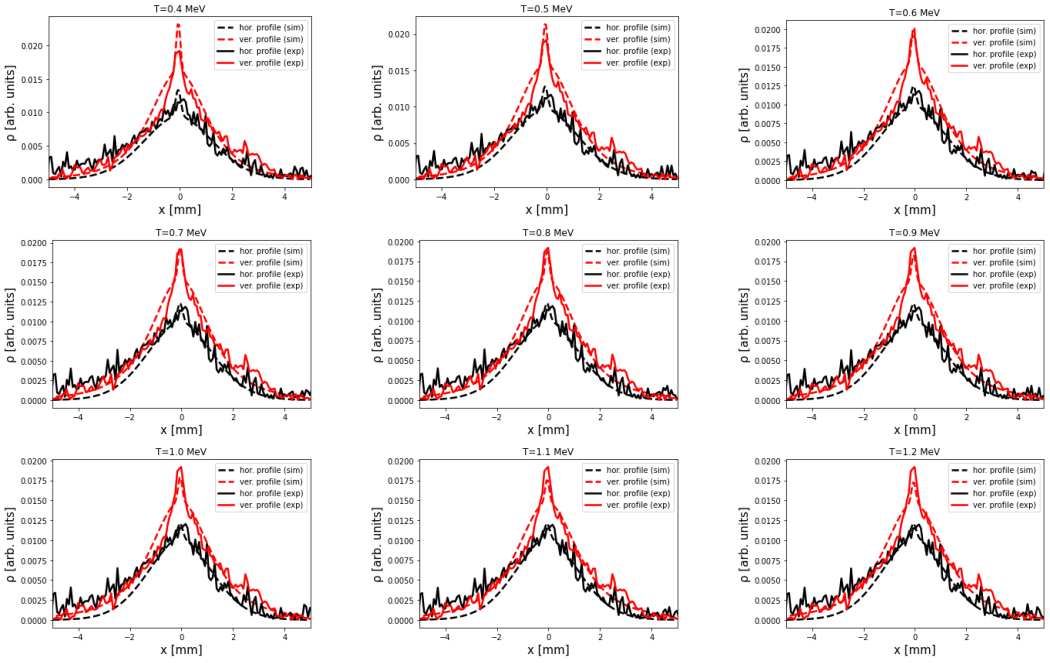

Figure 3. Comparison between experimental and calculated profiles for different beam temperatures. Best fit value: $T = 0.6$ MeV.

Consistent results have been found while measuring the beam temperature directly. The latter statement is confirmed by the comparisons shown in Figure 4. It is possible to see that the thermal representation of the spectrum lacks of precision around the proton cut-off energy region, as expected (a thermal distribution as the one in Equation (6) does not carry any information of a cut-off); however, the most of the protons passing through the quadrupole system are well represented by the same approximation. Indeed, the profile image shown in Figure 2 is dominated by the low-energy region of the proton spectrum since it contains most of the proton population. The spectral region of the plots in Figure 4 at low energies is limited by the acceptance of the detector. The reported spectra have been post-processed to account for the Pokalon effect and for the absorption in the scintillator. The high-energy cut-off is about 7 MeV for the following laser parameters: 25 J pulse energy, 30 fs pulse duration, and 15 µm spot size (FWHM) in the focal plane. The proton energy can be increased by a factor ∼3 stretching the laser pulse to few hundreds femtoseconds, but this was not the case during the described experiment.

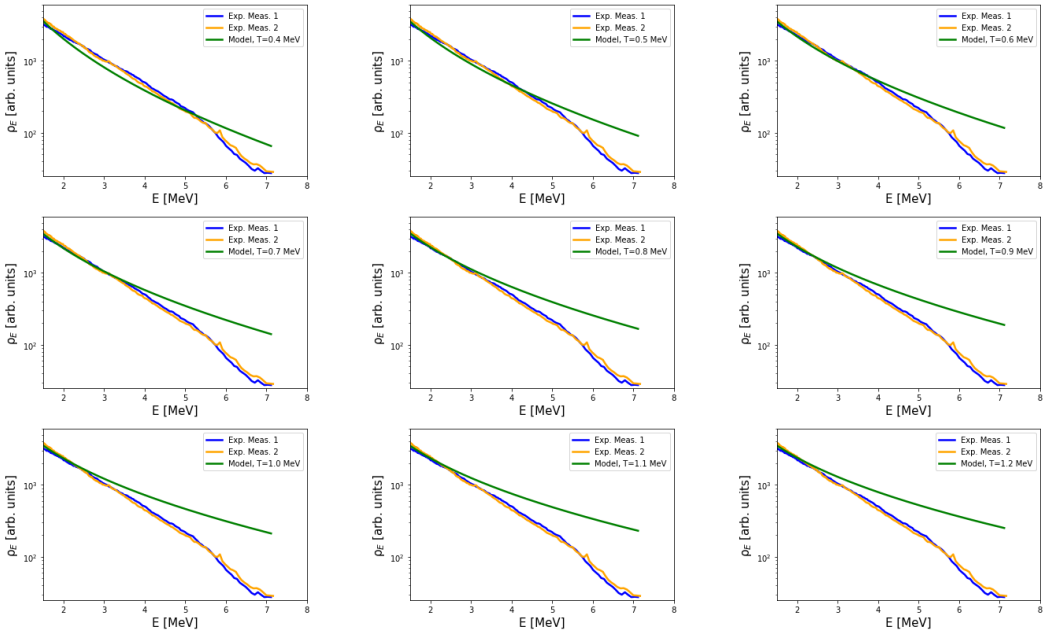

Figure 4. Comparison between experimental and calculated proton spectra for different beam temperatures. Best fit value: $T = 0.6$ MeV.

4. Discussion

We have demonstrated that the analytic solution of the Liouville equation, requiring computational time of the order of a fraction of a second, can be implemented for the study of transverse dynamics of particle beams along transport lines. We have adopted such a formalism for analyzing the case of a laser-proton beam. Figure 2 shows that the beam profile at the observation plane after the beam propagation from the source through a focusing system is in good agreement with measurements. Non-linear aberrations of the focusing system are not well-reproduced (the halos around the proton hot-spot are not exactly the same in the simulation compared to the measurement). This means that for a more detailed study, or better for achieving a higher degree of accuracy, a more sophisticated strategy may be needed as a particle tracker for example, or even a more precise choice of the particle trajectories in non-linear field maps within the same Liouville approach. However, particle trackers, even when used for relatively simple transport systems as the one considered in this paper, require from several minutes to tens of minutes to complete a calculation. This is basically due to the fact that in the presence of high losses, the number of particles to be followed in order to obtain a statistically representative sample at the end of the simulation is of the order of millions at least. The latter problem is bypassed by the Liouville approach that by definition follows all the particles at once. To have an idea of the losses induced by our transport system we present Figure 5.

In this figure, the integral of the trace-space density (normalized to one at the origin) is shown along the beamline. Due to the highly divergent source of ions, as well as broadband in kinetic energy, which is typical in a laser-plasma acceleration context, and also due to the quadrupole apertures (17 mm of radius, circular aperture), beam losses are unavoidable. At the end of the line the amount of charge transported has decreased by over two orders of magnitude. Nevertheless, by means of the results shown in Figure 5, it is possible to retrieve the amount of charge entering the focusing system. In fact, from an absolute calibration of the scintillator light vs. the proton flux, it has been possible to measure that the amount of charge transported to the detector is $\sim$20 pC. According the Liouville model of our beamline in terms of the result at Figure 5 we can then infer the amount of charge at the entrance of $Q1$, i.e., $\sim$3 nC.

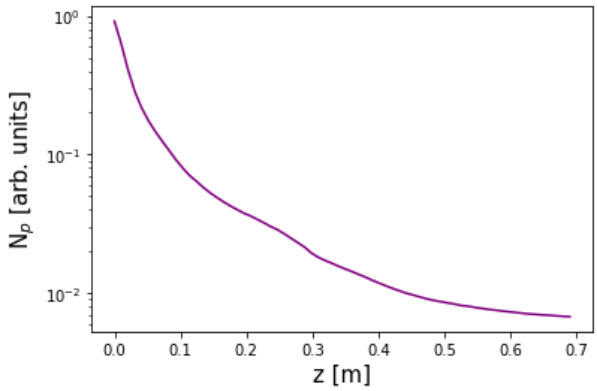

Figure 5. Beam losses along the transport line, i.e., number of transported protons N_p (normalized to 1 at the origin) calculated as integral of the phase space density.

5. Conclusions

The use of the analytic solution of the Liouville equation expressed in terms of exponential operators has been demonstrated as a powerful tool to study complex dynamical systems. The implementation of such approach to particle accelerators has been reported in the past for studying the temporal profile evolution of ultra-relativistic electron bunches in RF accelerators. In this paper we have generalized the approach for non-relativistic ion beams generated by laser-plasma accelerators. Such beams present wide distributions, which necessarily determine chromatic effects and losses in the transport lines after the generation point. Here, we have demonstrated not only that the Liouville approach can be a valid tool for reconstructing the envelope dynamics of the laser-accelerated particle beams passing through a focusing system, but also that it can be a powerful online tool for indirectly determining the beam temperature, i.e., the shape of the energy spectrum at least in the mostly populated region, far from the cut-off. The algorithm exploits the chromaticity of the system for associating a certain beam profile to a certain energy spectrum based on the minimization of the differences between the measured and calculated profiles at the observation plane. Moreover, the same approach allows a fast retrieval of the information on the bunch charge at the entrance of the transport system. The advantage of using the Liouville method instead of others (as particle trackers, for example) is that the solution of the Liouville equation is generated within a fraction of second, therefore it is a good candidate for online diagnostics and feedback in fast acquisition environments.

Author Contributions: Conceptualization, A.C.; software, A.C.; investigation, A.C., J.I.A.A., T.C.R., M.E., B.K., A.M., A.P.D., C.S.L., L.V. and G.G.; writing—original draft preparation, A.C.; writing—review and editing, A.C., J.I.A.A., T.C.R., M.E., B.K., A.M., A.P.D., C.S.L., L.V. and G.G.; visualization, A.C., J.I.A.A., T.C.R., M.E., B.K., A.M., A.P.D., C.S.L., L.V. and G.G.; supervision, G.G. All authors have read and agreed to the published version of the manuscript.

Funding: This publication is part of the grant CLP263P20, financed by the Ministry of Education of the Junta de Castilla y León, co-financed with FEDER funds.

Data Availability Statement: The data that support the findings of this study are available from the corresponding author on reasonable request.

Conflicts of Interest: The authors declare no conflict of interest.

Appendix A. Liouville Equation with Aperture Losses

Expressing the Liouville equation in full-derivative with respect to z, it is obtained:

$$\frac{d\rho_{\perp}^{E}}{dz} = \rho_{\perp}^{E} \frac{\partial \log A(x, y; z)}{\partial z} \tag{A1}$$

At this level the term on the right of the equation is a guess but we here demonstrate that is correct. In fact, the solution of Equation (A1) is:

$$\rho_{\perp}^{E} = A \times \rho_{\perp}^{E}\Big|_{A=1} \tag{A2}$$

The meaning of the above equation is evident: when $A = 1$, i.e., when there is no loss in the system, the phase-space density is conserved, as expected from the Liouville theorem. On the other hand, with losses, the phase space density is no longer constant during the evolution of the particle ensemble. From another point of view we may observe that in a conservative force field the Liouville operator at Equation (2) is unitary (hence the Liouville theorem) but in a dynamical system with losses the same operator undergoes the transformation $\hat{L} \to A \times \hat{L}$, with A being a function of the time and coordinates with absolute value $\lesssim 1$, which means that unitarity is lost.

Appendix B. Single-Particle Dynamics for the Case Relevant to This Paper

In this paper we study the proton transport along a beamline made by drifts and quadrupolar magnetic fields. For the drifts in free space each proton follows the trivial trajectory from an initial point z_i to a final point z_f:

$$\theta_{x,y}(z_f) = \theta_{x,y}(z_i) \tag{A3}$$

For the dynamics of the particles that pass inside the quadrupoles instead we obtain:

$$\theta_{x,y}(z_f) = \theta_{x,y}(z_i)\cos\left(\sqrt{\frac{\pm qg}{\sqrt{2ME}}}z_f\right) - \sqrt{\frac{\pm qg}{\sqrt{2ME}}}\{x,y\}(z_i)\sin\left(\sqrt{\frac{\pm qg}{\sqrt{2ME}}}z_f\right) \tag{A4}$$

It is straightforward to verify that, according to our previous definition of the force field, the positive sign in Equation (A4) must be chosen for Q_1 and Q_3 concerning the y-axis and for Q_2 concerning the x-axis, while the negative sign for all other cases. The single-particle dynamics along the full transport line is constructed piecewise using Equations (A3) and (A4) while imposing continuity conditions. The so-obtained $\theta_{x,y}(z)$ functions are plugged into Equation (5) together with the expression of the force field (please notice that $\{x,y\}(z) = \int_0^z \theta_{x,y}(z')dz'$). The trace-space density can be thus immediately calculated at any z-plane.

References

1. Brüning, O.; Rossi, L. (Eds.) *The High Luminosity Large Hadron Collider: The New Machine for Illuminating the Mysteries of Universe*; World Scientific Publishing Company: Singapore, 2015; Volume 24.
2. Muramatsu, M.; Kitagawa, A. A review of ion sources for medical accelerators. *Rev. Sci. Instrum.* **2012**, *83*, 02B909. [CrossRef]
3. Hamm, R.W.; Hamm, M.E. (Eds.) *Industrial Accelerators and Their Applications*; World Scientific Publishing Company: Singapore, 2012.
4. Amaldi, U. The importance of particle accelerators. *Europhys. News* **2000**, *31*, 5–9. [CrossRef]
5. Morabito, A.; Scisciò, M.; Veltri, S.; Migliorati, M.; Antici, P. Design and optimization of a laser-PIXE beamline for material science applications. *Laser Part. Beams* **2019**, *37*, 354–363. [CrossRef]
6. Macchi, A.; Borghesi, M.; Passoni, M. Ion acceleration by superintense laser-plasma interaction. *Rev. Mod. Phys.* **2013**, *85*, 751. [CrossRef]
7. Passoni, M.; Bertagna, L.; Zani, A. Target normal sheath acceleration: Theory, comparison with experiments and future perspectives. *New J. Phys.* **2010**, *12*, 045012. [CrossRef]
8. Apiñaniz, J.I.; Malko, S.; Fedosejevs, R.; Cayzac, W.; Vaisseau, X.; De Luis, D.; Gatti, G.; McGuffey, C.; Bailly-Grvaux, M.; Bhutwala, K.; Ospina-Bohorquez, V. A quasi-monoenergetic short time duration compact proton source for probing high energy density states of matter. *Sci. Rep.* **2021**, *11*, 6881. [CrossRef]
9. Chen, S.N.; Gauthier, M.; Higginson, D.P.; Dorard, S.; Mangia, F.; Riquier, R.; Atzeni, S.; Marquès, J.R.; Fuchs, J. Monochromatic short pulse laser produced ion beam using a compact passive magnetic device. *Rev. Sci. Instrum.* **2014**, *85*, 043504. [CrossRef]
10. Wu, M.; Zhu, J.; Li, D.; Yang, T.; Liao, Q.; Geng, Y.; Xu, X.; Li, C.; Shou, Y.; Zhao, Y.; Lu, Y. Collection and focusing of laser accelerated proton beam by an electromagnetic quadrupole triplet lens. *Nucl. Instrum. Methods Phys. Res. Sect. Accel. Spectrometers Detect. Assoc. Equip.* **2020**, *955*, 163249. [CrossRef]

11. Schollmeier, M.; Becker, S.; Geißel, M.; Flippo, K.A.; Blažević, A.; Gaillard, S.A.; Gautier, D.C.; Grüner, F.; Harres, K.; Kimmel, M.; Nürnberg, F. Controlled transport and focusing of laser-accelerated protons with miniature magnetic devices. *Phys. Rev. Lett.* **2008**, *101*, 055004. [CrossRef]
12. Br, i F.; Labate, L.; Palla, D.; Kumar, S.; Fulgentini, L.; Koester, P.; Baffigi, F.; Chiari, M.; Panetta, D.; Gizzi, L.A. A Few MeV Laser-Plasma Accelerated Proton Beam in Air Collimated Using Compact Permanent Quadrupole Magnets. *Appl. Sci.* **2021**, *11*, 6358. [CrossRef]
13. Burris-Mog, T.; Harres, K.; Nürnberg, F.; Busold, S.; Bussmann, M.; Deppert, O.; Hoffmeister, G.; Joost, M.; Sobiella, M.; Tauschwitz, A.; Zielbauer, B. Laser accelerated protons captured and transported by a pulse power solenoid. *Phys. Rev. Spec. Top.-Accel. Beams* **2011**, *14*, 121301. [CrossRef]
14. Masood, U.; Bussmann, M.; Cowan, T.E.; Enghardt, W.; Karsch, L.; Kroll, F.; Schramm, U.; Pawelke, J. A compact solution for ion beam therapy with laser accelerated protons. *Appl. Phys. B* **2014**, *117*, 41–52. [CrossRef]
15. Busold, S.; Schumacher, D.; Deppert, O.; Brabetz, C.; Frydrych, S.; Kroll, F.; Joost, M.; Al-Omari, H.; Blažević, A.; Zielbauer, B.; Hofmann, I. Focusing and transport of high-intensity multi-MeV proton bunches from a compact laser-driven source. *Phys. Rev. Spec. Top.-Accel. Beams* **2013**, *16*, 101302. [CrossRef]
16. Ter-Avetisyan, S.; Schnürer, M.; Polster, R.; Nickles, P.V.; Sandner, W. First demonstration of collimation and monochromatisation of a laser accelerated proton burst. *Laser Part. Beams* **2008**, *26*, 637–642. [CrossRef]
17. Kroll, F.; Brack, F.E.; Bernert, C.; Bock, S.; Bodenstein, E.; Brüchner, K.; Cowan, T.E.; Gaus, L.; Gebhardt, R.; Helbig, U.; Karsch, L. Tumour irradiation in mice with a laser-accelerated proton beam. *Nat. Phys.* **2022**, *18*, 316–322. [CrossRef]
18. Brown, A.; Suit, H. The centenary of the discovery of the Bragg peak. *Radiother. Oncol.* **2004**, *73*, 265–268. [CrossRef]
19. Flottmann, K.; Lidia, S.; Piot, P. *Recent Improvements to the ASTRA Particle Tracking Code (No. LBNL-52933)*; Lawrence Berkeley National Lab. (LBNL): Berkeley, CA, USA, 2003.
20. Borland, M. *Elegant: A Flexible SDDS-Compliant Code for Accelerator Simulation (No. LS-287)*; Argonne National Lab.: Argonne, IL, USA, 2000.
21. Curcio, A.; Panas, R.; Knafel, M.; Wawrzyniak, A.I. Liouville theory for fully analytic studies of longitudinal beam dynamics and bunch profile reconstruction in dispersive lines. *Nucl. Instrum. Methods Phys. Res. Sect. Accel. Spectrometers Detect. Assoc. Equip.* **2021**, *986*, 164755. [CrossRef]
22. Babusci, D.; Dattoli, G.; Quattromini, M.; Sabia, E. Relativistic harmonic oscillator, the associated equations of motion, and algebraic integration methods. *Phys. Rev. E* **2013**, *87*, 033202. [CrossRef]
23. Fuchs, J.; Antici, P.; d'Humières, E.; Lefebvre, E.; Borghesi, M.; Brambrink, E.; Cecchetti, C.A.; Kaluza, M.; Malka, V.; Manclossi, M.; et al. Laser-driven proton scaling laws and new paths towards energy increase. *Nat. Phys.* **2006**, *2*, 48–54. [CrossRef]
24. Volpe, L.; Fedosejevs, R.; Gatti, G.; Pérez-Hernández, J.A.; Méndez, C.; Apiñaniz, J.; Vaisseau, X.; Salgado, C.; Huault, M.; Malko, S.; et al. Generation of high energy laser-driven electron and proton sources with the 200 TW system VEGA 2 at the Centro de Laseres Pulsados. *High Power Laser Sci. Eng.* **2019**, *7*, e25. [CrossRef]
25. Salgado-López, C.; Apiñaniz, J.I.; Henares, J.L.; Pérez-Hernández, J.A.; de Luis, D.; Volpe, L.; Gatti, G. Angular-Resolved Thomson Parabola Spectrometer for Laser-Driven Ion Accelerators. *Sensors* **2022**, *22*, 3239. [CrossRef] [PubMed]